nature medicine

Resolution of inflammation by interleukin-9-producing type 2 innate lymphoid cells

Simon Rauber[1], Markus Luber[1], Stefanie Weber[1], Lisa Maul[1], Alina Soare[1], Thomas Wohlfahrt[1], Neng-Yu Lin[1], Katharina Dietel[1], Aline Bozec[1], Martin Herrmann[1], Mark H Kaplan[2], Benno Weigmann[3], Mario M Zaiss[1], Ursula Fearon[4], Douglas J Veale[5], Juan D Cañete[6], Oliver Distler[7], Felice Rivellese[8], Costantino Pitzalis[8], Markus F Neurath[3], Andrew N J McKenzie[9], StefanWirtz[3], Georg Schett[1], Jörg H W Distler[1] & Andreas Ramming[1]

Inflammatory diseases such as arthritis are chronic conditions that fail to resolve spontaneously. While the cytokine and cellular pathways triggering arthritis are well defined, those responsible for the resolution of inflammation are incompletely characterized. Here we identified interleukin (IL)-9-producing type 2 innate lymphoid cells (ILC2s) as the mediators of a molecular and cellular pathway that orchestrates the resolution of chronic inflammation. In mice, the absence of IL-9 impaired ILC2 proliferation and activation of regulatory T (T_{reg}) cells, and resulted in chronic arthritis with excessive cartilage destruction and bone loss. In contrast, treatment with IL-9 promoted ILC2-dependent T_{reg} activation and effectively induced resolution of inflammation and protection of bone. Patients with rheumatoid arthritis in remission exhibited high numbers of IL-9$^+$ ILC2s in joints and the circulation. Hence, fostering IL-9-mediated ILC2 activation may offer a novel therapeutic approach inducing resolution of inflammation rather than suppression of inflammatory responses.

Resolution of inflammation is still incompletely understood. In chronic inflammatory diseases, the physiological process of resolution of inflammation is impaired[1,2]. Diseases such as rheumatoid arthritis (RA) often start in young adulthood but fail to wane, requiring life-long immunosuppressive treatment[3]. Furthermore, the body's failure to effectively terminate inflammation leads to pronounced tissue damage such as bone loss[4,5]. Current treatment strategies for chronic inflammatory diseases like RA target proinflammatory cytokines and hence the activation process of inflammation, rather than promoting its resolution[6,7]. While lipid mediators such as resolvins have been implicated in resolution of inflammation[8], cytokine pathways governing this process are largely undefined thus far. Identification of such pathways, however, would allow rebalancing of inflammatory responses rather than generally suppressing inflammation and may substantially add to the development of new treatment possibilities. We were therefore interested in identifying novel pathways governing the resolution of arthritis. We identified IL-9 as a master regulator for resolution of arthritis and found that ILC2s, which produce IL-9, are essential for the initiation of this resolution process.

RESULTS

Antigen-induced arthritis (AIA) is a standard model of arthritis with spontaneous resolution (**Supplementary Fig. 1a**)[9,10]. In contrast, we observed that the course of AIA in *Il9*$^{-/-}$ mice was highly chronic (**Fig. 1a**). While joint swelling resolved spontaneously within 12–16 d in wild-type mice, it persisted beyond 42 d without signs of resolution in *Il9*$^{-/-}$ mice. The chronic inflammatory phenotype of *Il9*$^{-/-}$ mice was rescued by overexpression of IL-9 via hydrodynamic gene transfer (HDGT), using minicircle (MC) vectors encoding IL-9 (*Il9* MC) (**Fig. 1b**). Histological analysis of the affected knee joints of *Il9*$^{-/-}$ mice at day 42 confirmed persistent synovitis and demonstrated excessive degradation of cartilage and bone and higher numbers of osteoclasts as compared to wild-type mice (**Fig. 1c–e**). Microcomputed tomography showed pronounced loss of the trabecular network and bone volume as signs of inflammation-induced osteopenia in *Il9*$^{-/-}$ mice (**Fig. 1f**). In contrast to AIA, absence of IL-9 did not affect the course of acute inflammatory arthritis induced by monosodium urate crystals, which exclusively relies on neutrophil activation (**Supplementary Fig. 1b**).

Mice expressing the transgenic T cell receptor (TCR) KRN and the major histocompatibility complex (MHC) class II allele A^{g7} (K/BxN mice) develop autoantibodies against glucose-6-phosphate isomerase[11]. Passive transfer of serum from these mice is commonly used to initiate chronic arthritis (serum-transfer-induced arthritis, SIA)[12], with inflammation persisting over several weeks. To assess the therapeutic potential of IL-9 to promote its resolution, we overexpressed

[1]Department of Internal Medicine 3–Rheumatology and Immunology, Friedrich Alexander University Erlangen-Nürnberg (FAU) and Universitätsklinikum Erlangen, Erlangen, Germany. [2]Herman B Wells Center for Pediatric Research, Indianapolis, Indiana, USA. [3]Department of Internal Medicine 1, Friedrich Alexander University Erlangen-Nürnberg (FAU) and Universitätsklinikum Erlangen, Erlangen, Germany. [4]Molecular Rheumatology, School of Medicine, Trinity Biomedical Sciences Institute, Trinity College Dublin, Dublin, Ireland. [5]Centre for Arthritis and Rheumatic Diseases, St. Vincent's University Hospital, Dublin, Ireland. [6]Departamento de Reumatología, Hospital Clínic de Barcelona e IDIBAPS, Barcelona, Spain. [7]Division of Rheumatology, University Hospital Zurich, Zurich, Switzerland. [8]Centre for Experimental Medicine and Rheumatology, William Harvey Research Institute, Barts and the London School of Medicine and Dentistry, Queen Mary University of London and Barts Health NHS Trust, London, UK. [9]MRC Laboratory of Molecular Biology, Cambridge, UK. Correspondence should be addressed to A.R. (andreas.ramming@uk-erlangen.de).

Received 25 April; accepted 19 June; published online 17 July 2017; doi:10.1038/nm.4373

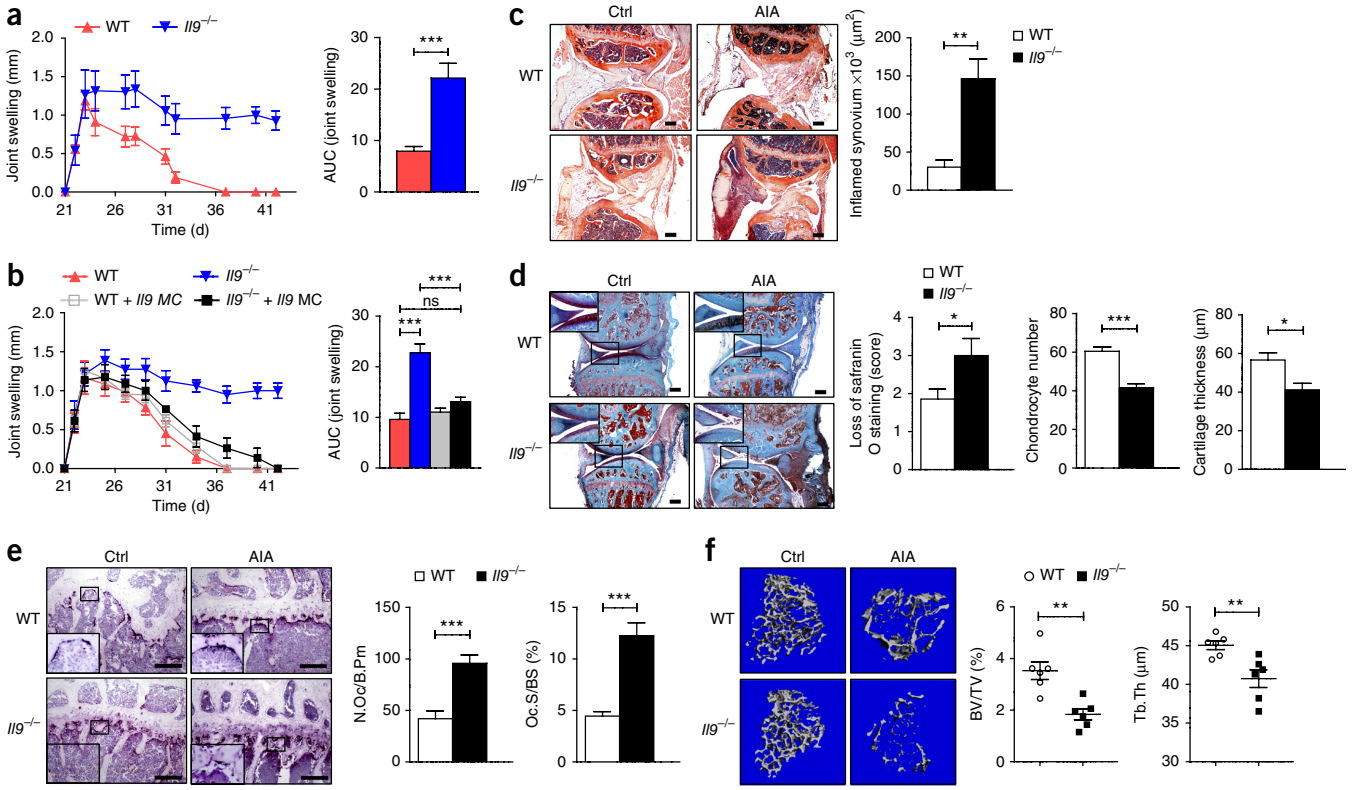

Figure 1 Chronic arthritis in *Il9*-deficient mice. (**a**) AIA in littermate wild-type (WT) ($n = 9$) and $Il9^{-/-}$ mice ($n = 7$) in three independent experiments; the *y* axes show knee swelling and the area under the curve (AUC) of knee swelling. (**b**) Overexpression of IL-9 by HDGT with MC encoding IL-9 in wild-type ($n = 7$) and $Il9^{-/-}$ ($n = 8$) mice at day 22 of AIA. Control minicircles (ctrl MC) were also injected into wild-type ($n = 6$) and $Il9^{-/-}$ ($n = 8$) mice. (**c**,**d**) Sections of knee joints from control (Ctrl) and AIA mice stained with H&E (**c**) or safranin O (**d**) at day 42 of AIA. Histomorphometric analysis ($n = 6$ each) was performed of the area of inflammation, proteoglycan loss, chondrocyte number and cartilage thickness. A representative image of each group is included. (**e**) Histomorphometric analysis of osteoclast numbers in the tibia of wild-type and $Il9^{-/-}$ mice ($n = 5$) at day 42 of AIA. A representative image of each group is included. N.Oc/B.Pm, number of osteoclasts per bone parameter; Oc.S/BS, osteoclast surface per bone surface. (**f**) Microcomputed tomography scans and assessment of microarchitectural parameters of tibial bone in control and AIA wild-type and $Il9^{-/-}$ mice ($n = 6$ for each group) at 14–16 weeks of age. BV/TV, bone volume per total volume; Tb.Th, trabecular thickness. Data are shown as mean ± s.e.m. Scale bars, 100 µm. $^{*}P < 0.05$, $^{**}P < 0.01$, $^{***}P < 0.001$, Student's *t* test (**a**, **c**–**f**) or one-way ANOVA with Tukey's *post hoc* test (**b**) for experiments including more than two groups in one experiment.

IL-9 using HDGT during the effector phase of SIA (3 d after induction of SIA). Consistent with our previous findings in AIA, overexpression of IL-9 did not have major effects on the initiation phase of SIA or on the maximal intensity of arthritis, but it strongly accelerated resolution (**Fig. 2a**). Joint swelling completely resolved within 9 d in mice with forced expression of IL-9, whereas arthritis in mice injected with the control vector was still worsening at day 9 (**Fig. 2a**,**b**). Histological analysis at day 9 showed substantially less synovitis in the paws of mice injected with *Il9* MC (**Fig. 2b**,**c**). Accelerated resolution of arthritis by IL-9 translated into reduced tissue damage with preservation of cartilage integrity, reduced osteoclast counts and decreased bone erosions (**Fig. 2b**–**e**).

To further characterize the mechanism by which IL-9 fosters the resolution of arthritis, the kinetics of pro- and anti-inflammatory mediators was analyzed in the serum and joints of arthritic $Il9^{-/-}$ and wild-type mice (**Fig. 3a** and **Supplementary Fig. 2a**,**b**). Time kinetics and concentrations of most key cytokine mediators such as tumor necrosis factor (TNF)-α, IL-6, interferon (IFN)-γ, IL-2 and IL-4 did not significantly differ between wild-type and $Il9^{-/-}$ mice. However, pronounced differences in IL-17 levels were observed, and these levels remained persistently high in $Il9^{-/-}$ AIA mice but returned to baseline levels in wild-type AIA mice. The selective upregulation of IL-17 was associated with enhanced T helper type 17 (T_H17) polarization, particularly in inflamed joints of $Il9^{-/-}$ mice, whereas naive, memory and effector T cell counts were comparable in wild-type and $Il9^{-/-}$ mice (**Fig. 3b**,**c**). These data demonstrate a shift to a persistent T_H17 cell–driven immune response in $Il9^{-/-}$ mice. To address the possibility that IL-9 serves as an intrinsic regulator of T_H17 differentiation, $CD4^+$ T cells from wild-type and $Il9^{-/-}$ mice were stimulated under T_H17-inducing conditions. Differentiation into conventional as well as inflammatory T_H17 cells was comparable in wild-type and $Il9^{-/-}$ mice (**Fig. 3d**), providing no evidence for an intrinsic defect in T_H17 development in $Il9^{-/-}$ mice but arguing for a central role of other cell types in the IL-9-induced inhibition of T_H17 polarization.

To identify these target cells of IL-9, we next analyzed regulatory T_{reg} cells in wild-type and $Il9^{-/-}$ mice at day 42 after immunization, when inflammation was resolved in wild-type mice but still persisted in $Il9^{-/-}$ mice. Total numbers of $CD4^+CD25^+Foxp3^+$ T_{reg} cells were comparable in $Il9^{-/-}$ and wild-type mice (**Fig. 3e**). However, the suppressive capacity of T_{reg} cells from $Il9^{-/-}$ mice was significantly decreased, as shown by coculture of CFSE-labeled $CD25^-Foxp3^-$ effector T (T_{eff}) cells with $Foxp3^+$ T_{reg} cells and subsequent analyses of proliferation of T_{eff} cells (**Fig. 3f**). The functional defect of $Il9^{-/-}$ T_{reg} cells was associated with significantly decreased

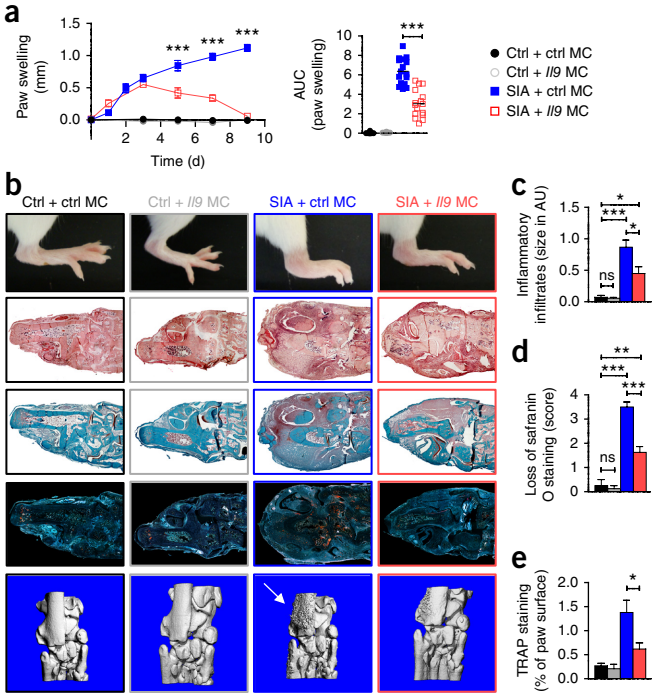

Figure 2 IL-9 accelerates the resolution of arthritis. (**a**) K/BxN SIA and non-arthritic (Ctrl) mice receiving HDGT with MC overexpressing IL-9 (*Il9* MC) (SIA, $n = 16$; Ctrl, $n = 10$) or control vector (SIA, $n = 16$; Ctrl, $n = 10$). The *y* axes show paw swelling and the AUC of paw swelling. (**b**) Representative images of paw swelling (line 1), H&E staining of joint tissue (line 2), safranin O staining (line 3), tartrate-resistant acid phosphatase (TRAP) staining (line 4) and microcomputed tomography (line 5) of the respective groups. The arrow highlights erosions. (**c**–**e**) Quantification of inflammation on H&E–stained sections (**c**), cartilage damage on safranin O–stained sections (**d**) and bone erosions on TRAP-stained sections (**e**). AU, arbitrary units. All data are shown as mean ± s.e.m. ns, $P > 0.05$; $^{*}P < 0.05$, $^{**}P < 0.01$, $^{***}P < 0.001$, one-way ANOVA with Tukey's *post hoc* test.

expression levels of functionally important effector molecules[13,14] such as GITR and ICOS in *Il9*$^{-/-}$ T_{reg} cells (**Fig. 3g**). To exclude the possibility that T_{eff} cells from *Il9*$^{-/-}$ mice are resistant to the effects of T_{reg} cells, the susceptibility of *Il9*$^{-/-}$ and wild-type T_{eff} cells to the suppressive effects of wild-type T_{reg} cells was assessed. Neither proliferation nor cytokine production differed between *Il9*$^{-/-}$ and wild-type responder T cells (**Fig. 3h**,**i**).

In line with previous reports, exogenous IL-9 modestly enhanced T_{reg} function *in vitro* (data not shown)[15]. However, prestimulation of T_{reg} cells from *Il9*$^{-/-}$ mice with IL-9 and adoptive transfer of these cells into *Il9*$^{-/-}$ mice did not prevent chronification of AIA (**Supplementary Fig. 3a**). We therefore further aimed to define cellular intermediates that might be involved in IL-9-induced resolution of inflammation. To explore the source of IL-9 in arthritis, AIA was induced in *Il9*^{citrine} reporter mice[16]. The majority of IL-9-producing cells did not express the lineage (Lin)-specific markers that define Lin^{+} lymphocytic and myeloid populations, including potential IL-9-producing cell types such as T helper type 9 (T_H9) cells[17–20] and mast cells[21] (**Fig. 4a**). More than 80% of the Lin^{-}citrine^{+} cells expressed ST2, ICOS (**Fig. 4a**), CD25, CD90 and Sca-1 (**Supplementary Fig. 3b**), suggesting that ILC2s are the predominant source of IL-9 during the resolution phase of arthritis, as defined as the segment of time between the peak of inflammation and 50% regression[22] (**Fig. 4a**).

These data were supported by quantitative analysis of synovial tissue sections from wild-type AIA mice stained with immunofluorescence-labeled antibodies. ILC2s were identified as the major source of IL-9 during resolution of AIA (**Supplementary Fig. 3c**). Furthermore, expression levels of mast cell–specific genes in inflamed joints did not differ between wild-type and *Il9*$^{-/-}$ mice (**Supplementary Fig. 3d**,**e**). ILC2 numbers were profoundly decreased in the synovium of *Il9*$^{-/-}$ mice (**Fig. 4b**). Impaired proliferation may account for the reduced numbers of ILC2s, as the number of proliferating Ki67^{+} ILC2s was significantly decreased in the arthritic knee joints of *Il9*$^{-/-}$ mice (**Fig. 4b**). In line with previous reports that IL-9 production by ILC2s acts in an autocrine loop to promote ILC proliferation[23,24], induction of ILC2s by overexpression of IL-25 and IL-33 using HDGT confirmed an intrinsic defect of ILC2 proliferation in *Il9*$^{-/-}$ mice (**Supplementary Fig. 4a**). Addition of IL-9 led to complete reconstitution of ILC2s. Confirming the relevance of this finding for the pathogenesis of chronic arthritis, multicolor immunofluorescence microscopy (IF) revealed that IL-9-producing ILC2s were located in close proximity to CD3^{+}Foxp3^{+} T_{reg} cells in the inflamed synovium (**Fig. 4c**). The colocalization of ILC2s and T_{reg} cells in the inflamed tissue supports the notion of cellular interactions that might be of functional relevance for T_{reg} suppression. Indeed, stimulation of ILC2s with IL-9 induced upregulation of the T_{reg}-receptor-associated ligands GITRL and ICOSL (**Fig. 4d**).

To determine the functional impact of interactions between ILC2s and T_{reg} cells, we performed T_{reg} suppression assays in the presence and absence of ILC2s. These assays demonstrated that ILC2s stimulated the suppressive capacity of T_{reg} cells. Whereas *Il9*$^{-/-}$ T_{reg} cells alone did not suppress T_{eff} proliferation, addition of ILC2s completely rescued this impaired suppressive capacity of *Il9*$^{-/-}$ T_{reg} cells (**Fig. 4e**). Transwell experiments revealed that these ILC2-mediated effects on *Il9*$^{-/-}$ T_{reg} cells required direct cell contacts (**Supplementary Fig. 4b**). Screening for potential mediators of this contact-dependent effect showed that ILC2s express high levels of GITRL and ICOSL, which are known to promote the suppressive capacity of T_{reg} cells[13,14]. Blockade of GITR–GITRL and ICOS–ICOSL interaction reversed the ILC2-mediated effects on the suppressive capacity of *Il9*$^{-/-}$ T_{reg} cells (**Fig. 4e**). Consistent with this model, ligand binding to GITR and ICOS on *Il9*$^{-/-}$ T_{reg} cells also restored the suppressive capacity of *Il9*$^{-/-}$ T_{reg} cells in the absence of ICOSL/GITRL-bearing ILC2s (**Fig. 4f**). *In vivo*, adoptive transfer of *Il9*$^{-/-}$ T_{reg} cells that had been preactivated via GITR and ICOS *ex vivo* led to these cells regaining their suppressive activity in the AIA model (**Fig. 4g**), highlighting that receptor–ligand specific interactions between ILC2s and T_{reg} cells activate the suppressive capacity of T_{reg} cells. To confirm the functional impact of ILC2s on the resolution of inflammation, ILC2s were adoptively transferred into *Il9*$^{-/-}$ mice with AIA. Adoptive transfer of ILC2s inhibited activation of T_H17 cells and promoted resolution of inflammation in *Il9*$^{-/-}$ mice (**Fig. 4h** and **Supplementary Fig. 4c**).

To investigate the role of IL-9 for the resolution of inflammation in humans, synovial tissues of patients with RA were analyzed as prototypical chronic inflammatory joint disease. In line with previous reports[25,26], the dominant part of IL-9 expression in the synovial membranes of patients with active RA came from Lin^{+} cells (**Fig. 5a**,**b**). Only low numbers of IL-9^{+} ILC2s were found in active RA, despite extensive synovial inflammation. In contrast, patients with RA in clinical remission exhibited high numbers of Lin^{-}IL-9^{+} ILC2s and a significant decline of Lin^{+}IL-9^{+} cells (**Fig. 5a**,**b**). Patients with acute joint inflammation after trauma demonstrated only a tendency toward increased numbers of Lin^{+}IL-9^{+} and Lin^{-}IL-9^{+} cells as

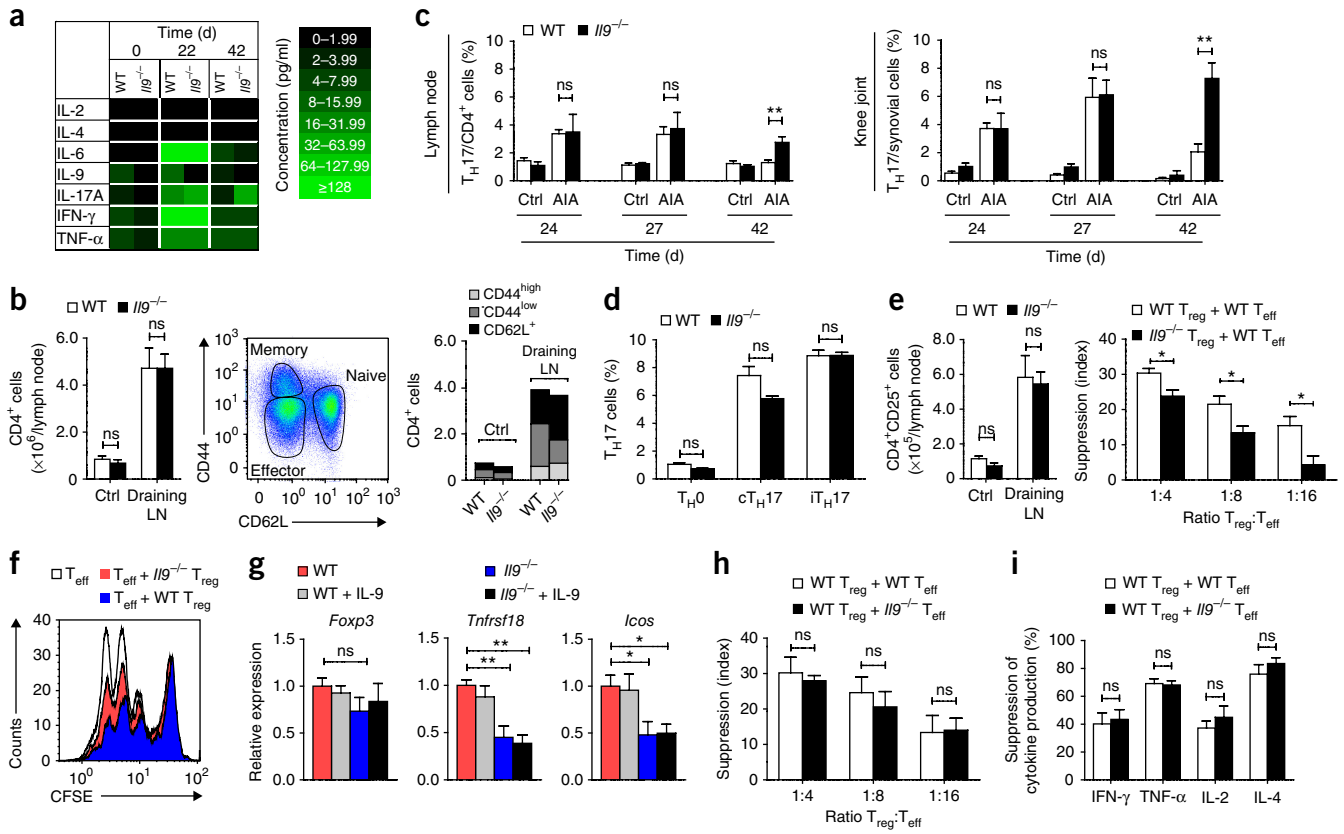

Figure 3 Altered T_H17 and T_{reg} responses in arthritic *Il9*$^{-/-}$ mice. (**a**) Heat map of serum levels of the indicated cytokines from AIA wild-type ($n = 3–6$) and *Il9*$^{-/-}$ ($n = 3–6$) littermates before immunization (day 0), after inoculation (day 22) and after resolution of inflammation in wild-type mice (day 42). (**b**) CD4$^+$ cell compartment in control and draining lymph nodes (LN) of AIA wild-type ($n = 5$) and *Il9*$^{-/-}$ ($n = 5$) mice analyzed for memory (CD44^{high}), effector (CD44^{low}) and naive (CD62L$^+$) T cells at day 42 of AIA. A representative dot plot is included. (**c**) T_H17 cells in control and draining lymph nodes and control and affected knee joints of AIA wild-type ($n = 3–7$) and *Il9*$^{-/-}$ ($n = 3–7$) mice assessed by flow cytometry at days 24, 27 and 42 of AIA. (**d**) Differentiation of CD4$^+$ T cells from wild-type ($n = 4$) and *Il9*$^{-/-}$ ($n = 4$) mice into conventional (cT_H17) and inflammatory (iT_H17) T_H17 cells. The T_H0-stimulating condition served as a control. (**e**) Quantification of CD4$^+$CD25$^+$Foxp3$^+$ T_{reg} cells in control and draining lymph nodes of AIA wild-type ($n = 5$) and *Il9*$^{-/-}$ ($n = 5$) mice at day 42 of AIA. (**f**) T_{reg} suppression assay: suppressive capacity of CD4$^+$CD25$^+$Foxp3$^+$ T_{reg} cells from wild-type ($n = 16$) and *Il9*$^{-/-}$ ($n = 17$) mice. Cell proliferation of CD4$^+$Foxp3$^-$ responder cells (T_{eff}) was assessed by dilution of the fluorescent dye CFSE into dividing daughter cells. Representative histograms are included. Suppression was calculated using the division index. (**g**) mRNA expression levels of Foxp3 and co-stimulatory receptors GITR (*Tnfrsf18*) and ICOS in sorted CD4$^+$CD25^{high}Foxp3$^+$ T_{reg} cells ($n = 4$ each) stimulated with anti-CD3/CD28 in the presence and absence of recombinant IL-9 for 48 h. (**h**) T_{reg} suppression assay: susceptibility of wild-type and *Il9*$^{-/-}$ ($n = 5$ each) T_{eff} cells to becoming suppressed by wild-type T_{reg} cells. (**i**) Wild-type T_{reg}-induced suppression of cytokines released from wild-type and *Il9*$^{-/-}$ T_{eff} cells ($n = 6$ each). All data are shown as the mean ± s.e.m. of 3–6 independent experiments of each group. ns, $P > 0.05$; $^*P < 0.05$, $^{**}P < 0.01$, $^{***}P < 0.001$, Student's *t* test (**b**–**f**, **h**, **i**) or ordinary one-way ANOVA with Tukey's *post hoc* test (**g**).

compared to healthy individuals. Longitudinal analysis of infiltrates in synovial tissue of patients with RA before and 6 months after the start of anti-inflammatory treatment showed a shift in the cellular source of IL-9 from Lin$^+$IL-9$^+$ cells during active disease to Lin$^-$IL-9$^+$ ILC2s 6 months later when antirheumatic drugs had led to remission of arthritis (**Fig. 5c**). Stratification of patients with RA according to disease activity revealed that ILC2 numbers in the blood were particularly low in patients with persistent inflammatory activity, but significantly higher in patients who were in disease remission (**Fig. 5d**,**e**). ILC2 numbers significantly correlated with disease activity in RA, as measured by standardized disease activity score 28 (DAS28) (**Fig. 5e**). Longitudinal observations of patients showed a reciprocal link between ILC2s and disease activity (**Fig. 5f**). These data, taken in combination with the results from the mouse models, indicate a pivotal role of ILC2s in the resolution of chronic inflammation and prevention of immunochronicity.

DISCUSSION

Our data demonstrate that IL-9 fosters resolution of inflammation and restores immune homeostasis in arthritis. IL-9 virtually exclusively affected the resolution phase of the disease, while only minor effects were observed in the induction phase. In some experiments, a tendency to higher peak inflammation was observed in IL-9-deficient mice, although these effects were only mild and were not consistent among the experiments. These observations may be explained by the regulatory action of IL-9 starting before the peak of inflammation has been reached. Nonetheless, induction of resolution clearly emerged as the primary action of IL-9 in arthritis, in contrast to the effects of other known cytokines involved in arthritis such as TNF-α, IL-6 and IL-17, which are primarily involved in the induction phase and which are successfully targeted by modern cytokine inhibitors. Our data show that resolution of arthritis is mechanistically based on the induction of ILC2s by IL-9, which in turn elicits GITR–GITRL- and

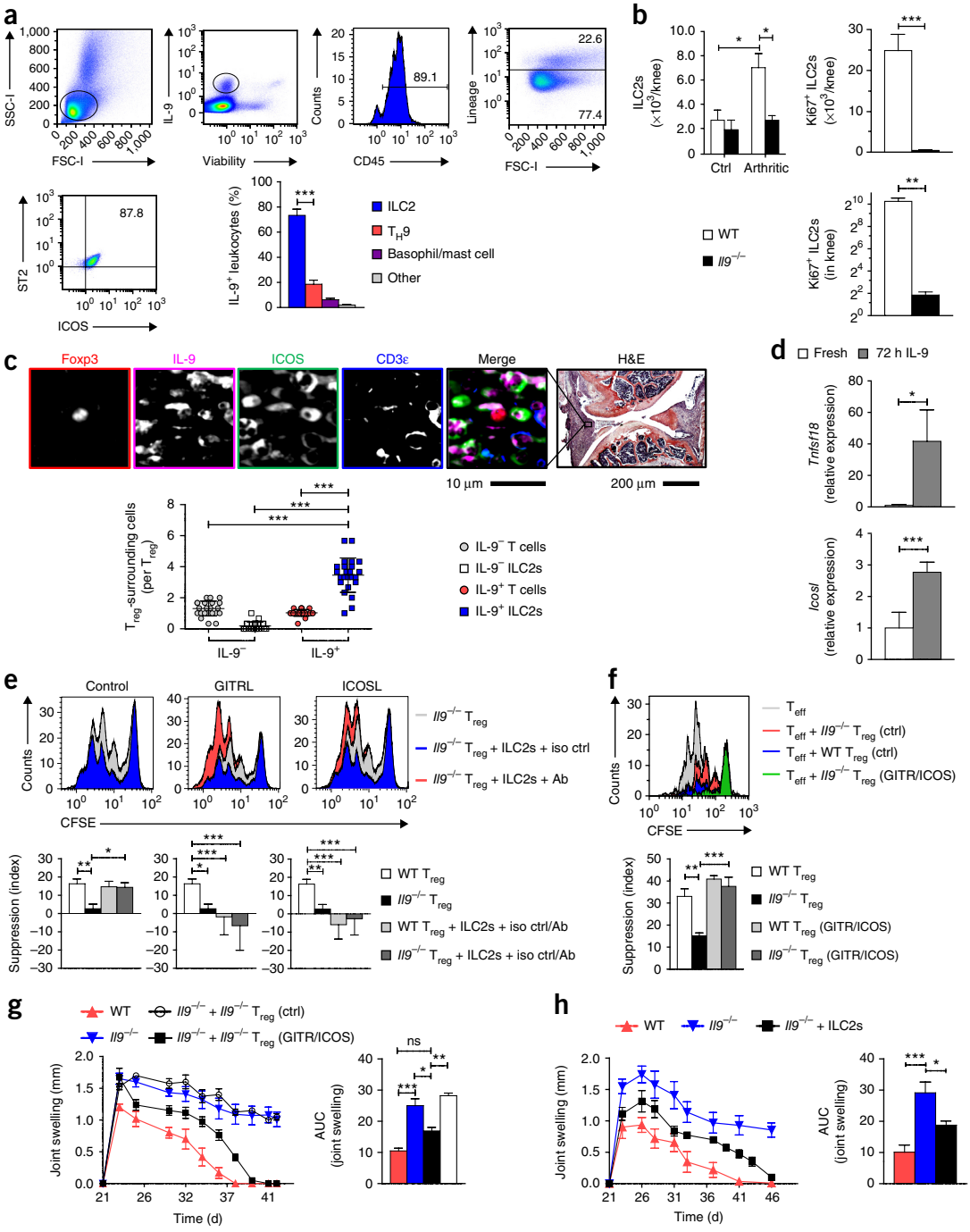

Figure 4 ILC2s sustain the suppressive capacity of T_{reg} cells by co-stimulation via ICOSL–ICOS and GITRL–GITR. (**a**) Flow cytometry analysis of AIA in *Il9*^{citrine} reporter mice ($n = 6$). Cells isolated from joints at day 27 were stratified according to viability, IL-9, CD45, lineage markers (Lin; CD3ε, CD11b, CD11c, CD45R, CD49b, FcER1a, Gr-1 and TER-119), ICOS and ST2. Representative plots are shown. (**b**) Quantification of ILC2s in control and arthritic joints from AIA wild-type and *Il9*$^{-/-}$ mice at day 27 ($n = 5$ each) by flow cytometry. Co-staining for Ki67 was performed to assess proliferation of ILC2s. (**c**) IF microscopy of inflamed joints of wild-type mice ($n = 4$) with AIA at day 27 stained for Foxp3, IL-9, ICOS and CD3ε. Randomly chosen T_{reg} cells from six tissue sections per mouse were analyzed for surrounding cells stratified by IL-9 production and surface markers. Data are shown as mean ± s.e.m. Representative images are shown. (**d**) mRNA expression levels of GITRL (*Tnfsf18*) and ICOSL in sorted ILC2s cultured in the presence or absence of recombinant IL-9 for 72 h ($n = 5$ each). (**e**,**f**) T_{reg} suppression assay: suppressive capacity of CD4$^+$Foxp3$^+$ T_{reg} cells from wild-type and *Il9*$^{-/-}$ mice. (**e**) Cocultures with ILC2s in the presence or absence of blocking antibodies (Ab) against GITRL or ICOSL ($n > 7$ each). (**f**) Prestimulation of *Il9*$^{-/-}$ T_{reg} cells with recombinant ICOSL and agonistic anti-GITR before coculture with responder cells (T_{eff}; $n = 4$ each). Isotype control (iso ctrl) antibody was used as a control. Representative histograms are included. Suppression was calculated using the division index. (**g**) *Il9*$^{-/-}$ T_{reg} cells were prestimulated *ex vivo* with recombinant ICOSL and agonistic anti-GITR before adoptive transfer into *Il9*$^{-/-}$ mice induced for AIA ($n > 4$ each). (**h**) ILC2s were adoptively transferred into *Il9*$^{-/-}$ mice induced for AIA ($n > 8$ each). The *y* axes show knee swelling and the AUC of knee swelling. All data are shown as the mean ± s.e.m. of three independent experiments of each group. ns, $P > 0.05$; $^*P < 0.05$, $^{**}P < 0.01$, $^{***}P < 0.001$, one-way ANOVA with Tukey's *post hoc* test (**a**–**c**, **e**–**h**) or Student's *t* test (**b**,**d**).

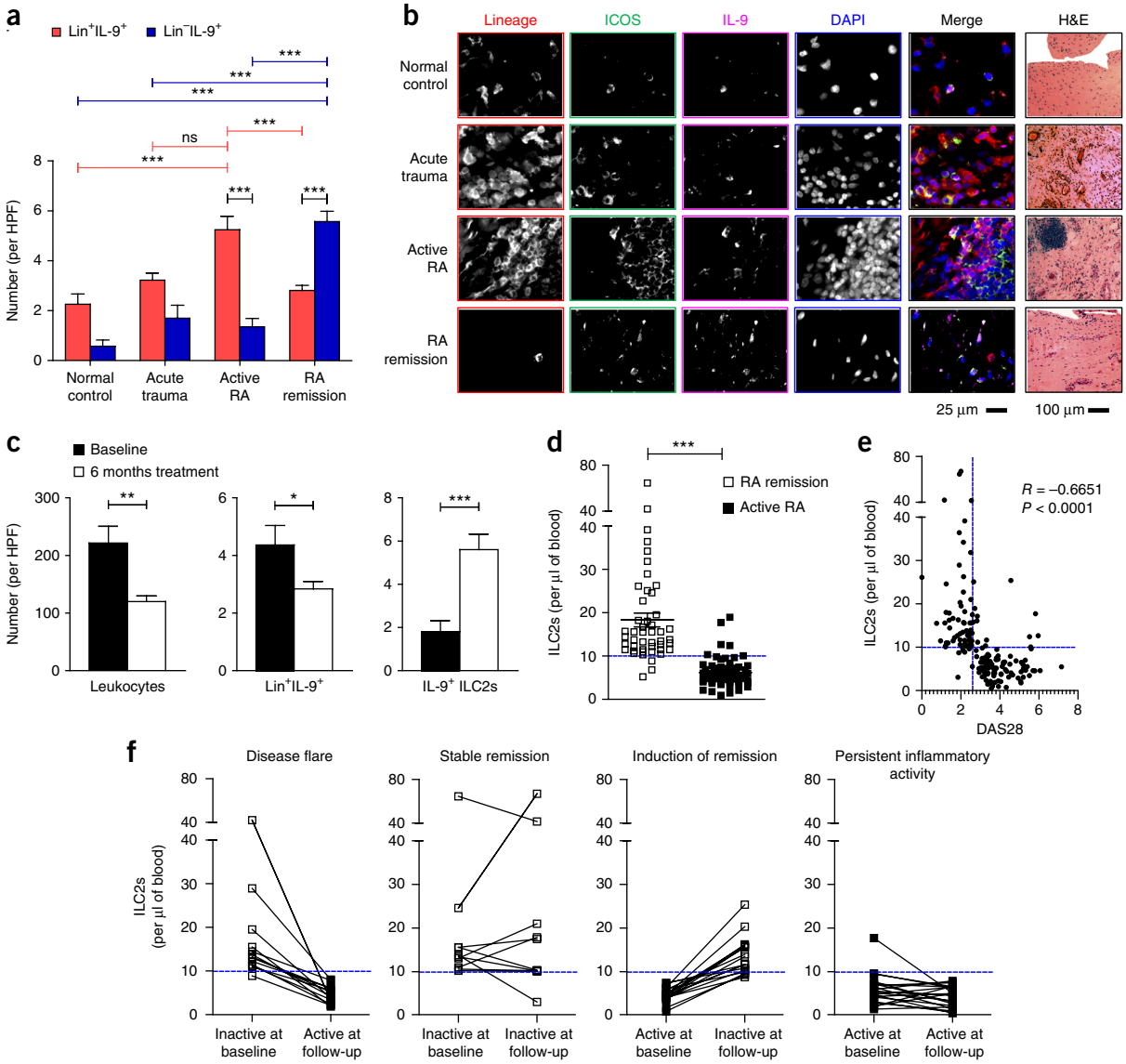

Figure 5 IL-9 during resolution of human arthritis. (**a**–**c**) IF microscopy of human synovial biopsies stained for lineage markers (Lin; CD3, CD11b, CD16 and mast cell tryptase), ICOS, IL-9 and DAPI. (**a**) Histomorphometric analysis was performed by quantification of $Lin^+IL\text{-}9^+$ and $Lin^-ICOS^+IL\text{-}9^+$ (ILC2) cells per 0.3 mm^2 of synovial tissue by five independent and blinded researchers. Data are shown as mean ± s.e.m. Included are normal controls ($n = 11$), patients with acute trauma ($n = 8$), patients with RA having active disease ($n = 19$; DAS28 score >3.2) and patients with RA in remission ($n = 19$; DAS28 score <2.6). (**b**) Representative IF images. (**c**) Quantification of Lin^+, $Lin^+IL\text{-}9^+$ and $Lin^-ICOS^+IL\text{-}9^+$ (ILC2) cells in patients with RA with high disease activity (DAS28 score = 5.1 ± 1.2; $n = 10$) before and after 6 months of treatment with antirheumatic drugs inducing disease remission. HPF, high-power field. (**d**–**f**) Absolute counts of ILC2s in the blood of patients with RA ($n = 111$). (**d**) ILC2 counts in patients with active disease (DAS28 score ≥3.2; $n = 61$) and inactive disease (DAS28 score <2.6; $n = 50$); data are shown as mean ± s.e.m. (**e**) Correlation between ILC2 counts and DAS28 score; the correlation analysis used was nonparametric (Spearman's correlation). (**f**) Longitudinal observation of ILC2 counts at baseline and follow-up 6–12 months later in patients with RA ($n = 63$) stratified into four groups according to baseline and follow-up disease activity (inactive versus active). $^*P < 0.05$, $^{**}P < 0.01$, $^{***}P < 0.001$, one-way ANOVA with Tukey's *post hoc* test (**a**) or Student's *t* test (**c**, **d**).

ICOS–ICOSL-dependent activation of T_{reg} cells. This IL-9-mediated forced resolution of arthritis translates into reduced tissue damage such as bone and cartilage loss, which usually result from chronic inflammation in the context of arthritis. Our data provide evidence that IL-9 has a dichotomous function in different phases of inflammation. Previous studies have shown that under certain circumstances IL-9 can promote inflammation in acute models[15,16,27,28]. In chronic arthritis, however, IL-9 acts as a cytokine governing the resolution phase of the disease. These findings are remarkable, as resolution of inflammation has thus far been preferentially attributed to lipid mediators such as resolvins and little was known about innate/adaptive immune system interactions in orchestrating the resolution process[2]. IL-9 and the function of ILC2s in this process provide strong support for the existence of immune pathways that primarily foster the resolution of inflammation and restore immune homeostasis in chronic inflammatory diseases. From a therapeutic perspective, such approaches are highly attractive, as they provide an anchor to allow rebalancing of the pathological inflammatory response in the

near future rather than exposing patients to broad suppression of inflammatory responses.

METHODS

Methods, including statements of data availability and any associated accession codes and references, are available in the online version of the paper.

Note: Any Supplementary Information and Source Data files are available in the online version of the paper.

ACKNOWLEDGMENTS

The authors thank M. Pascual, K. Dreissigacker, R. Kleinlein, M. Comazzi, D. Weidner and B. Happich for excellent technical assistance. We thank U. Appelt and M. Mroz of the Core Unit Cell Sorting and Immunomonitoring Erlangen for cell sorting. This work was supported by the Deutsche Forschungsgemeinschaft (RA 2506/3-1 and RA 2506/4-1 to A.R.; DI 1537/5-1, DI 1537/7-1, DI 1537/8-1, DI 1537/9-1, AK 144/2-1 and DI 1537/11-1 to J.H.W.D.; SCHE 1583/7-1 to G.S.; SPP1468-IMMUNOBONE and CRC1181 to G.S. and J.H.W.D.), the Bundesministerium für Bildung und Forschung (METHARTHROS to G.S. and J.H.W.D.), the Marie Curie project OSTEOIMMUNE (to G.S. and J.H.W.D.), the TEAM project of the European Union and the IMI-funded project RTCure (to G.S.), Else Kröner-Fresenius-Stiftung 2014_A184 (to A.R.), the Wilhelm Sander Foundation (2013.056.1 to J.H.W.D.), the Interdisciplinary Centre for Clinical Research, Erlangen (A64 to J.H.W.D.; J40 to A.R.), the ELAN Fonds of the Universitätsklinikum Erlangen (16-10-05-1 to A.R.), the Career Support Award of Medicine of the Ernst Jung Foundation (to J.H.W.D.), SNF Sinergia CRSII3_154490 (to O.D.), the UK MRC (UI015178805; to A.N.J.M.), the Wellcome Trust (100963/Z/13/Z to A.N.J.M.) and US NIH grant AI057459 (to M.H.K.).

AUTHOR CONTRIBUTIONS

Design of the study: S.R., G.S., J.H.W.D., A.R. Acquisition of data: S.R., M.L., S. Weber, L.M., A.S., T.W., N.-Y.L., K.D., M.G., A.R. Interpretation of data: S.R., A.B., M.H., A.N.J.M., B.W., M.M.Z., U.F., D.J.V., J.D.C., O.D., F.R., C.P., S. Wirtz, M.F.N., G.S., J.H.W.D., A.R. Support of material: A.B., M.H., M.H.K., B.W., U.F., D.J.V., J.D.C., O.D., F.R., C.P., M.F.N., A.N.J.M., S. Wirtz. Manuscript preparation: S.R., G.S., J.H.W.D., A.R.

COMPETING FINANCIAL INTERESTS

The authors declare no competing financial interests.

1. Nathan, C. & Ding, A. Nonresolving inflammation. *Cell* **140**, 871–882 (2010).
2. Buckley, C.D., Gilroy, D.W., Serhan, C.N., Stockinger, B. & Tak, P.P. The resolution of inflammation. *Nat. Rev. Immunol.* **13**, 59–66 (2013).
3. McInnes, I.B. & Schett, G. The pathogenesis of rheumatoid arthritis. *N. Engl. J. Med.* **365**, 2205–2219 (2011).
4. Kotas, M.E. & Medzhitov, R. Homeostasis, inflammation, and disease susceptibility. *Cell* **160**, 816–827 (2015).
5. Schett, G. & Gravallese, E. Bone erosion in rheumatoid arthritis: mechanisms, diagnosis and treatment. *Nat. Rev. Rheumatol.* **8**, 656–664 (2012).
6. Steinman, L., Merrill, J.T., McInnes, I.B. & Peakman, M. Optimization of current and future therapy for autoimmune diseases. *Nat. Med.* **18**, 59–65 (2012).
7. Schett, G., Elewaut, D., McInnes, I.B., Dayer, J.M. & Neurath, M.F. How cytokine networks fuel inflammation: toward a cytokine-based disease taxonomy. *Nat. Med.* **19**, 822–824 (2013).
8. Serhan, C.N., Chiang, N. & Van Dyke, T.E. Resolving inflammation: dual anti-inflammatory and pro-resolution lipid mediators. *Nat. Rev. Immunol.* **8**, 349–361 (2008).
9. Kehoe, O., Cartwright, A., Askari, A., El Haj, A.J. & Middleton, J. Intra-articular injection of mesenchymal stem cells leads to reduced inflammation and cartilage damage in murine antigen-induced arthritis. *J. Transl. Med.* **12**, 157 (2014).
10. Brackertz, D., Mitchell, G.F. & Mackay, I.R. Antigen-induced arthritis in mice. I. Induction of arthritis in various strains of mice. *Arthritis Rheum.* **20**, 841–850 (1977).
11. Monach, P.A., Mathis, D. & Benoist, C. The K/BxN arthritis model. *Curr. Protoc. Immunol.* Chapter 15, Unit 15.22 (2008).
12. Kollias, G. *et al.* Animal models for arthritis: innovative tools for prevention and treatment. *Ann. Rheum. Dis.* **70**, 1357–1362 (2011).
13. Ji, H.B. *et al.* Cutting edge: the natural ligand for glucocorticoid-induced TNF receptor–related protein abrogates regulatory T cell suppression. *J. Immunol.* **172**, 5823–5827 (2004).
14. Stephens, G.L. *et al.* Engagement of glucocorticoid-induced TNFR family–related receptor on effector T cells by its ligand mediates resistance to suppression by $CD4^+CD25^+$ T cells. *J. Immunol.* **173**, 5008–5020 (2004).
15. Elyaman, W. *et al.* IL-9 induces differentiation of T_H17 cells and enhances function of $FoxP3^+$ natural regulatory T cells. *Proc. Natl. Acad. Sci. USA* **106**, 12885–12890 (2009).
16. Gerlach, K. *et al.* T_H9 cells that express the transcription factor PU.1 drive T cell–mediated colitis via IL-9 receptor signaling in intestinal epithelial cells. *Nat. Immunol.* **15**, 676–686 (2014).
17. Kaplan, M.H., Hufford, M.M. & Olson, M.R. The development and *in vivo* function of T helper 9 cells. *Nat. Rev. Immunol.* **15**, 295–307 (2015).
18. Dardalhon, V. *et al.* IL-4 inhibits TGF-β-induced $Foxp3^+$ T cells and, together with TGF-β, generates $IL\text{-}9^+$ $IL\text{-}10^+$ $Foxp3^-$ effector T cells. *Nat. Immunol.* **9**, 1347–1355 (2008).
19. Veldhoen, M. *et al.* Transforming growth factor-β 'reprograms' the differentiation of T helper 2 cells and promotes an interleukin 9–producing subset. *Nat. Immunol.* **9**, 1341–1346 (2008).
20. Ramming, A., Druzd, D., Leipe, J., Schulze-Koops, H. & Skapenko, A. Maturation-related histone modifications in the PU.1 promoter regulate Th9-cell development. *Blood* **119**, 4665–4674 (2012).
21. Lu, L.F. *et al.* Mast cells are essential intermediaries in regulatory T-cell tolerance. *Nature* **442**, 997–1002 (2006).
22. Bannenberg, G.L. *et al.* Molecular circuits of resolution: formation and actions of resolvins and protectins. *J. Immunol.* **174**, 4345–4355 (2005).
23. Wilhelm, C. *et al.* An IL-9 fate reporter demonstrates the induction of an innate IL-9 response in lung inflammation. *Nat. Immunol.* **12**, 1071–1077 (2011).
24. Turner, J.E. *et al.* IL-9-mediated survival of type 2 innate lymphoid cells promotes damage control in helminth-induced lung inflammation. *J. Exp. Med.* **210**, 2951–2965 (2013).
25. Ciccia, F. *et al.* Potential involvement of IL-9 and Th9 cells in the pathogenesis of rheumatoid arthritis. *Rheumatology* **54**, 2264–2272 (2015).
26. Kundu-Raychaudhuri, S., Abria, C. & Raychaudhuri, S.P. IL-9, a local growth factor for synovial T cells in inflammatory arthritis. *Cytokine* **79**, 45–51 (2016).
27. Chang, H.C. *et al.* The transcription factor PU.1 is required for the development of IL-9-producing T cells and allergic inflammation. *Nat. Immunol.* **11**, 527–534 (2010).
28. Nowak, E.C. *et al.* IL-9 as a mediator of Th17-driven inflammatory disease. *J. Exp. Med.* **206**, 1653–1660 (2009).

ONLINE METHODS

Experimental approaches. Experiments were not performed in a blinded fashion except when specifically indicated. There were no exclusion criteria for the human and animal experiments. Mice were stratified according to sex and then randomized into the different groups. Cells from human donors were also randomized.

Mice. Wild-type BALB/cJRj female mice were purchased from Janvier. BALB/c *Il9*$^{-/-}$ mice[29] and *Il9*^{citrine} reporter mice[16] were bred in house. *Foxp3*^{GFP} reporter mice (C.Cg-*Foxp3*^{tm2Tch}/J) were purchased from Jackson Labs and backcrossed on BALB/c *Il9*$^{-/-}$ mice to generate *Il9*$^{-/-}$ × *Foxp3*^{GFP} reporter mice. CD45.1 mice were kindly provided by D. Mielenz (Nikolaus Fiebiger Center). All mice were bred under specific-pathogen-free conditions, and all studies were approved by the animal ethical committee of the government of Unterfranken, Würzburg, Germany.

Patient characteristics. For synovial tissue analyses (ILC2, IL-9-expressing cells), samples from untreated patients with active RA (n = 19) and patients with RA in remission receiving treatment with disease-modifying antirheumatic drugs (methotrexate, n = 15; TNF inhibitors, n = 5) were analyzed (n = 19). Samples were retrieved by synovial biopsy in centers from Barcelona, Dublin and Erlangen, Germany. Subjects with RA fulfilled the 2010 American College of Rheumatology (ACR) classification criteria for RA[30]. Remission was defined by a DAS28 of less than 2.6 (ref. 31). There was no significant difference in sex distribution (65.0% versus 73.7%), age distribution (52.3 ± 19.8 years versus 52.9 ± 18.2 years), rheumatoid factor status (67.4% versus 63.1%) and status of antibodies to citrullinated protein (58.5% versus 68.4%) between the two groups. Disease activity in the active RA group was 5.8 ± 1.4 according to DAS28, while it was 1.9 ± 0.5 in the remission group.

In addition, a longitudinal biopsy cohort of ten patients with early RA (disease duration of <12 months) from London undergoing synovial biopsies at baseline and 6 months after the start of antirheumatic therapy was analyzed. 70% were females, the mean age was 49.8 ± 22.6 years, and 70% had rheumatoid factor or antibodies to citrullinated protein. Disease activity at baseline was 5.1 ± 1.2 and at follow-up was 2.0 ± 0.6. Patients received treatment with either methotrexate monotherapy or a combination of methotrexate and/or sulfasalazine and/or hydroxychloroquine. For control purposes, synovial tissue from patients with acute trauma (n = 8) resembling acute inflammation after joint injury were investigated. In addition, normal synovium was used as control tissue, which was obtained from surgery specimens of patients with no articular disease process (n = 11). Written informed consent was obtained from all subjects. The study was approved by the ethical committee of the University of Erlangen-Nürnberg.

For the analysis of circulating ILC2s, a cohort of 111 patients with RA was analyzed. 73.9% were females, the mean age was 59.9 ± 14.3 years and the mean disease activity was 3.2 ± 1.3 according to DAS28. With respect to autoantibody status, 69.4% were positive for rheumatoid factor and 59.5% were positive for antibodies to citrullinated protein. With respect to antirheumatic treatment, 56.8% were treated with methotrexate and 28.8% were treated with biological antirheumatic drugs, mostly TNF inhibitors. 63 of these 111 patients received a follow-up assessment of circulating ILC2s 6 to 12 months after baseline assessment.

Assessment of circulating ILC2s in human blood. Venous human blood was collected with a standard collection system and EDTA as anticoagulant (Sarstedt). The collected blood was processed for routine automated complete blood count. Furthermore, 500 µl of whole blood was directly incubated with the fluorochrome-labeled antibodies listed in **Supplementary Table 1**. Following incubation with antibodies, red blood cells were lysed and nucleated cells were fixed using RBC Lysis and Fixation Solution (BioLegend). Flow cytometry was performed on a 3-laser/10-channel flow cytometer system (Navios, CE-licensed, Beckman Coulter) and analyzed using Beckman's proprietary software Kaluza, version 1.5. The gating strategy is shown in **Supplementary Figure 4d**. Frequencies of ILC2s (SSC^{low}CD45^{+}Lin^{-}IL7Ra^{+}cKIT^{-}CRTH2^{+}) were calculated as the percentage of lymphocytes (SSC^{low}CD45^{high}). Absolute numbers of cells were calculated as follows: % ILC2s × absolute lymphocyte count (automated count) = absolute number of ILC2s per mm^{3}.

Antigen-induced arthritis and clinical evaluation. Mouse AIA was induced in female littermates of the stated background that were aged 8 to 10 weeks. Mice were immunized with a booster injection 7 d after by subcutaneous injections with 100 µg of methylated BSA (mBSA) in 100 µl of an emulsion with equal amounts of PBS and complete Freund's adjuvant (all from Sigma-Aldrich). As additional adjuvant, 5 × 10^{8} heat-inactivated whole *Bordetella pertussis* (NIBSC) were administrated intraperitoneally in 100 µl of PBS. 21 d after the initial immunization, mouse AIA was induced in the right knee joint by intra-articular inoculation of 100 µg of mBSA in 25 µl of PBS. The same volume of PBS without mBSA was injected into mice serving as controls. In cases of adoptive transfer of ILC2s, 5 × 10^{3} sorted ILC2s were administrated by intra-articular injection together with 100 µg of mBSA in 25 µl of PBS. In a subset of experiments, ILC2s were sorted from CD45.1 mice to verify survival and that ILC2s remained within the knee joint (**Supplementary Fig. 4e**). For adoptive transfer of T_{reg} cells, T_{reg} cells were sorted as CD4^{+}CD25^{high} cells using non-depleting clones. For some experiments, T_{reg} cells were concentrated to 1 × 10^{6} cells/ml and pre-incubated with recombinant mouse IL-9 (50 ng/ml; Immunotools) or a combination of recombinant mouse ICOSL (1 µg/ml; Abcam) and agonistic antibody to GITR (10 µg/ml; clone DTA-1, BioLegend) in complete IMEM overnight. 0.5 × 10^{6} T_{reg} cells were adoptively transferred by intravenous injection in 100 µl of Ringer's solution. Animals were inspected every second day for arthritis development, and knee joint diameters were measured using a digital micrometer (Kroeplin). The difference in joint diameter measured before and after inoculation was used as a quantitative measure of swelling (in mm). In a subset of experiments, mice underwent HDGT with *Il9* MC DNA 1 d after inoculation (day 22).

Serum-transfer-induced arthritis and clinical evaluation. Female mice aged 8 weeks on the BALB/cJRj background were induced for SIA by a single intraperitoneal injection of 150 µl of serum generated from the F_1 generation of mice expressing the transgenic TCR KRN crossed onto mice bearing the MHC class II allele Ag7 (K/BxN mice). Serum from these mice is characterized by high serum titers of antibodies against the glycolytic enzyme glucose-6-phosphate isomerase. Animals were inspected every second day for arthritis development, and clinical parameters were monitored, including swelling of the paws and knees and body weight, by a researcher blinded to mouse treatment. Paw and knee swelling is expressed as the difference in paw and joint diameter measured (in mm) before and after injection of serum. Serum was collected for analysis before HDGT, 3 d after HDGT (2 d before serum transfer), and 3 and 9 d after serum transfer.

Injection of monosodium urate crystals as an acute inflammation model. The acute inflammation model has been described elsewhere[32]. Briefly, monosodium urate (MSU) crystals were produced by adjusting a solution of 10 mM uric acid and 154 mM NaCl (both from Merck KGaA) to pH 7.2 and shaking it for 3 d. The resulting crystals were washed in ethanol, dried under sterile conditions, sterilized at 180 °C for 2 h and stored in PBS (pH 7.0). For induction of the acute gout model, 1.5 mg of MSU in 50 µl of PBS was injected subcutaneously into the foot pads of wild-type and *Il9*$^{-/-}$ mice. Contralateral foot pads received an injection of 50 µl of PBS serving as a control. Animals were inspected at the indicated time points for paw swelling by a researcher blinded to mouse treatment.

Hydrodynamic gene transfer for induction of ILC2s and IL-9 overexpression. The principle of HDGT by tail vein injection allowing non-viral introduction of naked foreign plasmid DNA into hepatocytes has been described elsewhere[33,34]. Briefly, for HDGT, 10 µg of plasmid DNA was applied by tail vein injection into 1 volume of Ringer lactate-free solution corresponding to 10.5% of mouse body weight. For induction of ILC2s, plasmids encoding mouse IL-33 (ref. 35) and mouse IL-25 (a kind gift from S. Wirtz) were injected. Mice were sacrificed 60 h after HDGT to isolate ILC2s by flow cytometry–based cell sorting. All plasmids were isolated from their bacterial expression systems using the Invitrogen maxi prep kit (Thermo Fisher Scientific). To ensure efficient endotoxin removal, plasmid DNA was treated with Miraclean endotoxin removal kits (MirusBio). HDGT with *Il9* MC DNA was performed on day 22 in the AIA model and 5 d before serum transfer in the SIA model.

Protein concentrations in serum, tissue extracts and cell culture supernatants. Tissue extracts, serum samples and cell culture supernatants were

analyzed for secreted cytokines by a flow cytometry–based immune multiplex ELISA (BioLegend) following the instructions in the manufacturer's protocol on a 3-laser/10-channel flow cytometry system (Gallios, Beckman Coulter) and analyzed using Beckman's proprietary software Kaluza version 1.5. IL-9 and IL-33 serum levels were measured by ELISA kits purchased from BioLegend; an IL-25 ELISA kit was purchased from eBioscience. To determine the concentration of cytokines in knees during AIA, mouse knees were homogenized in a non-denaturing protein extraction buffer (100 mM Tris, pH 7.4, 150 mM NaCl, 1 mM EGTA, 1 mM EDTA, 1% Triton X-100, 0.5% sodium deoxycholate, 1 mM PMSF, 1% protease inhibitor cocktail (Sigma-Aldrich)) using the Precellys Ceramic Kit 2.8 mm on a tissue homogenizer (Peqlab). After homogenization, samples were subsequently centrifuged (18,000*g*, 20 min, 4 °C) to remove debris. Samples were aliquotted and frozen at −80 °C until analysis by ELISA.

Histological analyses and histomorphometry. Hind legs were fixed overnight in 4% formalin, skin and muscles were rigorously removed and bones were decalcified in 500 mM acid-free EDTA (Sigma-Aldrich) at 4 °C until bones were pliable. Decalcified and paraffin-embedded tibial bones and joints were cut in 5-µm sections and, following deparaffinization and rehydration by standard protocols, stained with H&E, safranin O or TRAP, using a leukocyte acid phosphatase staining kit (Sigma-Aldrich). Safranin O staining was performed according to a standard protocol (IHC world). Loss of safranin O staining was scored as follows: 0, normal; 1, slight reduction; 2, moderate reduction; 3, severe reduction; 4, no dye noted. Synovial inflammation, cartilage destruction and osteoclast numbers were quantified with a Zeiss Axioskop 2 microscope (Carl Zeiss) equipped with the OsteoMeasure system (Osteometrics) as described elsewhere[36]. Representative panorama images were reconstructed using the ImageJ distribution Fiji[37,38] augmented with the TurboReg[39] and MosaicJ[40] plugins. Scorings and quantifications were performed with blinding to sample identity.

Microcomputed tomography imaging and analysis. Structures of tibial bones and paws were measured with a SCANCO Medical µCT 40 scanner and analyzed with SCANCO evaluation software for segmentation, 3D morphometric analysis, density and distance parameters (SCANCO Medical).

Fluorescence imaging. Epitopes were retrieved from deparaffinized sections using a heat-induced method. Briefly, sections were alternately bathed in boiling sodium citrate buffer (10 mM sodium citrate, pH 6.0) and Tris-EDTA buffer (10 mM Tris base, 1 mM EDTA, 0.05% Tween-20, pH 9.0). Each bathing step was repeated five times for 2 min each. Sections were washed in distilled water and blocked for 1 h in PBS supplemented with 5% BSA and 2% horse serum. Sections were incubated with primary antibodies overnight at 4 °C and with secondary antibodies and DAPI after an intense washing step for 2 h at ambient temperature. Consecutive staining was performed to minimize cross-reactivity. Cross-reactivity was blocked by preincubation with species-specific immunoglobulin. The antibodies used are listed in **Supplementary Table 2**. Human synovial samples were stained for DAPI, CD3/CD11b/CD16/mast cell tryptase, ICOS and IL-9. Mouse synovial samples were stained for DAPI or Foxp3, ICOS, IL-9 and CD3ε. Sections were finally mounted in fluorescence mounting medium (Dako) and sealed with commercial nail polish. Images were acquired on a Nikon Eclipse 80i fluorescence microscope (Nikon).

Cell isolation for flow cytometry and cell sorting. Mice were sacrificed by cervical dislocation and dissected to generate single-cell suspensions from secondary lymphoid organs (SLOs) and synovial tissue. Fat was thoroughly removed from the dissected SLOs, and their capsules were opened to ensure good drainage of the digestive solution (digestion medium) consisting of RPMI-1640 medium supplemented with 0.4 mg/ml collagenase D from *Clostridium histolyticum* and 0.2 mg/ml DNase I, grade II, from bovine pancreas (both from Roche Diagnostics). For flow cytometry, single cutaneous lymph nodes were digested in 1 ml of digestion medium at 37 °C for 1 h on a thermoshaker at 1,000 r.p.m. (Eppendorf). Pipetting every 20 min ensured good dissociation of the tissue. Spleens and mesenteric lymph nodes were digested in proportionally higher volumes. The resulting single-cell suspension was filtered through a 70-µm cell strainer and washed in a larger volume of RPMI-1640 medium supplemented with 10 mM EDTA and 10% FCS (stop medium). To generate single-cell suspension from synovial tissue for flow cytometry analysis, whole legs were dissected and muscles and tendons were thoroughly removed. It was especially ensured that popliteal lymph nodes were removed. The femur and tibia were cut proximal to the knee joint, leaving fragments not longer than a few millimeters. The knee joint was then opened and digested twice for 1 h in 2 ml of enriched digestion medium containing 1 mg/ml collagenase D and 0.2 mg/ml DNase I. The resulting single-cell suspensions after 1 and 2 h were filtered through a 70-µm cell strainer and washed in a larger volume of stop medium. For sorting of lymphoid cells from spleen and mesenteric lymph nodes, the dissected SLOs of one mouse were pooled and digested four times in 3 ml of normal digestion medium for 15–20 min for each digestion. Pipetting before each exchange of the digestion medium ensured good dissociation of the cells. The collected single-cell suspensions were filtered through a 70-µm cell strainer and washed in a larger volume of stop medium. In all cases, RBCs were lysed after digestion by applying self-made ACK buffer for 1.5 min. Lysis was stopped by adding 10× PBS to generate 1× solution. Cells were then washed in PBS supplemented with 5 mM EDTA and 2% FCS and filtered through a 40-µm cell strainer.

***In vitro* polarization of T helper cells.** For *in vitro* generation of T_H1, T_H2, T_H9 and T_H17 cells, single-cell suspensions from spleen were generated as described above. $CD4^+$ T cells were enriched using a negative-selection magnetic enrichment kit (BioLegend). 1×10^6 $CD4^+$-enriched splenocytes were cultured in 48-well plates precoated with antibody to CD3ε (5 µg/ml; 200 µl/well for >1 h at 37 °C; clone 145-2C11) for 72 h at 37 °C in a humidified atmosphere containing 5% CO_2. The standard culture medium was IMDM medium supplemented with streptomycin (100 µg/ml), penicillin G (100 U/ml), amphotericin B (0.25 µg/ml), L-glutamine (2 mM; all from Gibco, Life Technologies), β-mercaptoethanol (0.5 mM) and 10% FCS. For undirected activation (T_H0), medium only was supplemented with antibody to CD28 (3 µg/ml; clone 37.51). For T_H1 differentiation, medium was supplemented with antibody to CD28 (3 µg/ml), antibody to IL-4 (10 µg/ml; clone 11B11) and IL-12 (20 ng/ml); for T_H2 differentiation medium was supplemented with antibody to CD28 (3 µg/ml), antibody to IFN-γ (10 µg/ml; clone AN-18) and IL-4 (10 ng/ml). For T_H9 differentiation, supplements included antibody to CD28 (3 µg/ml), antibody to IFN-γ (10 µg/ml; clone AN-18), TGF-β (5 ng/ml) and IL-4 (10 ng/ml). For conventional T_H17 differentiation, medium was supplemented with antibody to CD28 (3 µg/ml), antibody to IFN-γ (10 µg/ml), antibody to IL-4 (10 µg/ml), TGF-β (5 ng/ml) and IL-6 (20 ng/ml). For inflammatory T_H17 differentiation, medium was supplemented with antibody to CD28 (3 µg/ml), antibody to IFN-γ (10 µg/ml), antibody to IL-4 (10 µg/ml), TGF-β (5 ng/ml), IL-6 (100 ng/ml), IL-23 (30 ng/ml), IL-1β (20 ng/ml) and IL-21 (20 ng/ml). All cytokines and antibodies were purchased from BioLegend. For flow cytometry analysis, cells were restimulated with 81 nM phorbol 12-myristate 13-acetate (PMA) and 1.3 µM ionomycin in the presence of 5 ng/ml brefeldin A and 2 nM monensin (all from BioLegend) for 5 h.

Staining of single-cell suspensions for flow cytometry. For flow cytometry analysis, 1×10^6 cells were stained in a V-shaped 96-well microtiter plate. All antibodies and DAPI were diluted in PBS supplemented with 5 mM EDTA and 2% FCS. 100 µl of staining solution was used per well. Fixable viability dye was diluted in serum-free PBS as stated in the manufacturer's protocol. For cytoplasmic staining of cytokines, before staining, single-cell suspensions were stimulated for 5 h as described above. The intracellular fixation and permeabilization buffer set (eBioscience) was used as recommended in the manufacturer's instructions. For intranuclear staining of Foxp3 and Ki67, the Foxp3 staining buffer set (eBioscience) was used as recommended in the manufacturer's instructions. Concentrations of antibodies and other staining reagents are listed in **Supplementary Table 3**. Flow cytometry data were acquired on a 3-laser/10-channel flow cytometer system (Gallios, Beckman Coulter) and analyzed using Beckman's proprietary software Kaluza, version1.5.

Staining of single-cell suspensions for sorting. For sorting of T cell and ILC2 populations from SLOs, single-cell suspensions were concentrated to 40×10^6 cells/ml and staining was performed in PBS supplemented with 5 mM EDTA and 2% FCS. Cells were sorted with a jet-in air system (MoFlow Astrios, Beckman Coulter) equipped with a 70-µm nozzle at the Core Unit of Cell Sorting and Immunomonitoring, Friedrich Alexander University (FAU) Erlangen-Nürnberg.

doi:10.1038/nm.4373

Regulatory T cell sorting and restimulation. A single-cell suspension from spleen was prepared as described above. Cells were stained for CD25 and CD4 after blocking CD16/CD32 Fc-γ receptors as described above. T_{reg} cells were sorted as the $CD4^+CD25^{high}$ population. Foxp3 expression in T_{reg} cells was ensured by flow cytometry reanalysis. Sorted T_{reg} cells were cultured in RPMI-1640 medium supplemented with streptomycin (100 µg/ml), penicillin G (100 U/ml), amphotericin B (0.25 µg/ml), L-glutamine (2 mM; all from Gibco, Life Technologies) and 10% FCS. Medium was further supplemented with recombinant human IL-2 (200 ng/ml; BioLegend) and in some cases with recombinant mouse IL-9 (50 ng/ml; Immunotools). To ensure activation of T_{reg} cells, 1.25×10^5 cells were cultured in 96-well U-shaped plates together with beads coated with antibody to CD3 and CD28 (Dynabeads, Invitrogen) in a cell-to-bead ratio of 1:2. RNA was isolated as described below directly after sorting or after indicated time points of culture.

Suppression assays. Single-cell suspensions from spleens of *Foxp3*^{GFP} reporter or *Il9*$^{-/-}$ × *Foxp3*^{GFP} reporter mice were prepared as described above. Cells were stained for CD4 after blocking CD16/CD32 Fc-γ receptors as described above. T_{reg} cells were sorted as the $CD4^+GFP^+$ population. Responder T_{eff} cells were sorted as the $CD4^+GFP^-$ population. 10×10^6 wild-type T_{eff} cells were labeled with 1 ml of 1 µM CFSE (Thermo Fisher Scientific) for 8 min at 37 °C. Labeling was stopped by adding 2 volumes of FCS and washing cells twice in PBS supplemented with 5 mM EDTA and 2% FCS. 25×10^4 labeled wild-type T_{eff} cells were cocultured with unlabeled wild-type or *Il9*$^{-/-}$ T_{reg} cells in different ratios as indicated in U-shaped 96-well plates. Activation of T cells was achieved using beads coated with antibody to CD3 and CD28 (Dynabeads, Invitrogen) in a T_{eff}-to-bead ratio of 8:1. Culture medium was IMDM supplemented as for T cell differentiation but additionally contained 200 ng/ml recombinant human IL-2 (BioLegend). In some experiments, the standard protocol was modified and 25×10^4 sorted ILC2s were added to the coculture or ILC2s were cocultured in 96 HTS Transwell systems (Corning). Furthermore, some experiments were performed in the presence of recombinant mouse IL-9 at 50 ng/ml (Immunotools), antibody to GITRL at 10 µg/ml (clone 5F1, BioLegend) or antibody to ICOSL at 10 µg/ml (clone HK5.3, BioLegend), recombinant mouse ICOSL at 1 µg/ml (Abcam) and 10 µg/ml agonistic antibody to GITR (clone DTA-1, BioLegend). After 72 h of coculture, supernatants were collected and cells were isolated, washed, stained for TCRβ to distinguish ILC2s from T cells and analyzed by flow cytometry. Fluorescence signals of the CFSE reporter and endogenous GFP expression were distinguished by their different qualities of spillover. Cell proliferation was assessed by dilution of the fluorescent dye CFSE into dividing daughter cells, and suppression was calculated using the division index (DI); T_{eff} cells cultured alone served as the reference: suppression (index) = $100 - DI_{probe}/DI_{reference} \times 100$.

ILC2 sorting and restimulation. Pooled single-cell suspensions from spleen and mesenteric lymph nodes were generated from mice that received IL-25 and IL-33 plasmids via HDGT. Cell suspensions were stained after blocking CD16/CD32 Fc-γ receptors. ILC2s were identified as the $CD3\varepsilon^-B220^-CD49b^-FcERIa^-CD11b^-CD11c^-$ population expressing $KLRG1^{high}ICOS^{high}$. Sorted ILC2s were cultured in IMDM medium supplemented as for T cell differentiation but in the presence of 50 ng/ml recombinant mouse IL-9 (Immunotools) for 72 h. RNA was isolated as described below.

Gene expression analysis. Total RNA was extracted from single-cell suspensions using the Nucleo Spin RNA isolation kit (Macherey-Nagel). 1 µg of RNA was used to transcribe mRNA to cDNA following standard protocols. Real-time PCR was performed in triplicate using SYBR Green master mix (Applied Biosystems). Expression of target genes was calculated by the ΔCt comparative method for relative quantification after normalization. The endogenous control for T cells and whole tissue was β2 microglobulin and for sorted ILC2s was hypoxanthine guanine phosphoribosyl transferase (HPRT1). Primer sequences are listed in **Supplementary Table 4**.

Statistical analysis. Results were visualized and analyzed with Prism version 6 (GraphPad Software) and are depicted as mean ± s.e.m. if not stated otherwise. For two-group comparisons, a two-sided unpaired Student's *t* test was applied if the pretest for normality (D'Agostino–Pearson normality test) was not rejected at the 0.05 significance level; $P \leq 0.05$ was considered statistically significant. When two groups of samples were compared for iterating parameters or more than two groups of samples were compared, one-way ANOVA was used. Tukey's range test was used as *post hoc* analysis of ANOVA. Significance levels are indicated as suggested by Prism Software: ns, $P > 0.05$, $^*P \leq 0.05$, $^{**}P \leq 0.01$, $^{***}P \leq 0.001$. No statistical method was used to predetermine sample size.

A **Life Sciences Reproducibility Summary** for this paper is available.

Data availability. Supporting data can be obtained from the authors upon reasonable request. Source data are available online for **Figures 1–5**.

29. Townsend, J.M. *et al.* IL-9-deficient mice establish fundamental roles for IL-9 in pulmonary mastocytosis and goblet cell hyperplasia but not T cell development. *Immunity* **13**, 573–583 (2000).
30. Aletaha, D. *et al.* 2010 rheumatoid arthritis classification criteria: an American College of Rheumatology/European League Against Rheumatism collaborative initiative. *Ann. Rheum. Dis.* **69**, 1580–1588 (2010).
31. Prevoo, M.L. *et al.* Modified disease activity scores that include twenty-eight-joint counts. Development and validation in a prospective longitudinal study of patients with rheumatoid arthritis. *Arthritis Rheum.* **38**, 44–48 (1995).
32. Schauer, C. *et al.* Aggregated neutrophil extracellular traps limit inflammation by degrading cytokines and chemokines. *Nat. Med.* **20**, 511–517 (2014).
33. Liu, F., Song, Y. & Liu, D. Hydrodynamics-based transfection in animals by systemic administration of plasmid DNA. *Gene Ther.* **6**, 1258–1266 (1999).
34. Zhang, G., Budker, V. & Wolff, J.A. High levels of foreign gene expression in hepatocytes after tail vein injections of naked plasmid DNA. *Hum. Gene Ther.* **10**, 1735–1737 (1999).
35. McHedlidze, T. *et al.* Interleukin-33-dependent innate lymphoid cells mediate hepatic fibrosis. *Immunity* **39**, 357–371 (2013).
36. Lin, N.Y. *et al.* Autophagy regulates TNFα-mediated joint destruction in experimental arthritis. *Ann. Rheum. Dis.* **72**, 761–768 (2013).
37. Schneider, C.A., Rasband, W.S. & Eliceiri, K.W. NIH Image to ImageJ: 25 years of image analysis. *Nat. Methods* **9**, 671–675 (2012).
38. Schindelin, J. *et al.* Fiji: an open-source platform for biological-image analysis. *Nat. Methods* **9**, 676–682 (2012).
39. Thevenaz, P., Ruttimann, U.E. & Unser, M. A pyramid approach to subpixel registration based on intensity. *IEEE Trans. Image Process.* **7**, 27–41 (1998).
40. Thévenaz, P. & Unser, M. User-friendly semiautomated assembly of accurate image mosaics in microscopy. *Microsc. Res. Tech.* **70**, 135–146 (2007).

nature research

Corresponding author(s): Andreas Ramming

☐ Initial submission ☐ Revised version ☒ Final submission

Life Sciences Reporting Summary

Nature Research wishes to improve the reproducibility of the work that we publish. This form is intended for publication with all accepted life science papers and provides structure for consistency and transparency in reporting. Every life science submission will use this form; some list items might not apply to an individual manuscript, but all fields must be completed for clarity.

For further information on the points included in this form, see Reporting Life Sciences Research. For further information on Nature Research policies, including our data availability policy, see Authors & Referees and the Editorial Policy Checklist.

Experimental design

1. Sample size

Describe how sample size was determined.

Estimated necessary sample sizes were biometrically determined.

2. Data exclusions

Describe any data exclusions.

no data were excluded from the analysis

3. Replication

Describe whether the experimental findings were reliably reproduced.

Experimental findings were reliably reproduced in at least three independent experiments.

4. Randomization

Describe how samples/organisms/participants were allocated into experimental groups.

Mice were stratified according to sex and then randomized into the different groups. Cells from human donors were also randomized.

5. Blinding

Describe whether the investigators were blinded to group allocation during data collection and/or analysis.

Experiments were done in a blinded fashion except when specifically indicated.

Note: all studies involving animals and/or human research participants must disclose whether blinding and randomization were used.

6. Statistical parameters

For all figures and tables that use statistical methods, confirm that the following items are present in relevant figure legends (or in the Methods section if additional space is needed).

n/a	Confirmed
☐	☒ The exact sample size (*n*) for each experimental group/condition, given as a discrete number and unit of measurement (animals, litters, cultures, etc.)
☐	☒ A description of how samples were collected, noting whether measurements were taken from distinct samples or whether the same sample was measured repeatedly
☐	☒ A statement indicating how many times each experiment was replicated
☐	☒ The statistical test(s) used and whether they are one- or two-sided (note: only common tests should be described solely by name; more complex techniques should be described in the Methods section)
☐	☒ A description of any assumptions or corrections, such as an adjustment for multiple comparisons
☐	☒ The test results (e.g. *P* values) given as exact values whenever possible and with confidence intervals noted
☐	☒ A clear description of statistics including central tendency (e.g. median, mean) and variation (e.g. standard deviation, interquartile range)
☐	☒ Clearly defined error bars

See the web collection on statistics for biologists for further resources and guidance.

Nature Medicine: doi:10.1038/nm.4373

Software

Policy information about availability of computer code

7. Software

Describe the software used to analyze the data in this study.	Prim version 6 GraphPad Software, La Jolla, USA

For manuscripts utilizing custom algorithms or software that are central to the paper but not yet described in the published literature, software must be made available to editors and reviewers upon request. We strongly encourage code deposition in a community repository (e.g. GitHub). *Nature Methods* guidance for providing algorithms and software for publication provides further information on this topic.

Materials and reagents

Policy information about availability of materials

8. Materials availability

Indicate whether there are restrictions on availability of unique materials or if these materials are only available for distribution by a for-profit company.	All unique materials used are readily available from the authors or from standard commercial sources.

9. Antibodies

Describe the antibodies used and how they were validated for use in the system under study (i.e. assay and species).	Respective data are provided in supplementary tables.

10. Eukaryotic cell lines

a. State the source of each eukaryotic cell line used.	No eukaryotic cell line was used.
b. Describe the method of cell line authentication used.	No eukaryotic cell line was used.
c. Report whether the cell lines were tested for mycoplasma contamination.	No eukaryotic cell line was used.
d. If any of the cell lines used are listed in the database of commonly misidentified cell lines maintained by ICLAC, provide a scientific rationale for their use.	No commonly misidentified cell lines were used.

Animals and human research participants

Policy information about studies involving animals; when reporting animal research, follow the ARRIVE guidelines

11. Description of research animals

Provide details on animals and/or animal-derived materials used in the study.	Details on animals and animal-derived materials are described in Online-Methods.

Policy information about studies involving human research participants

12. Description of human research participants

Describe the covariate-relevant population characteristics of the human research participants.	Population characteristics of the human research participants are given in Online-Methods.

Nature Medicine: doi:10.1038/nm.4373

nature research

Corresponding author(s): Andreas Ramming

☐ Initial submission ☐ Revised version ☒ Final submission

Flow Cytometry Reporting Summary

Form fields will expand as needed. Please do not leave fields blank.

Data presentation

For all flow cytometry data, confirm that:

☒ 1. The axis labels state the marker and fluorochrome used (e.g. CD4-FITC).

☒ 2. The axis scales are clearly visible. Include numbers along axes only for bottom left plot of group (a 'group' is an analysis of identical markers).

☒ 3. All plots are contour plots with outliers or pseudocolor plots.

☒ 4. A numerical value for number of cells or percentage (with statistics) is provided.

Methodological details

5. Describe the sample preparation.	described in Material and Methods in detail
6. Identify the instrument used for data collection.	described in Material and Methods in detail
7. Describe the software used to collect and analyze the flow cytometry data.	described in Material and Methods (Kaluza software)
8. Describe the abundance of the relevant cell populations within post-sort fractions.	described in Material and Methods in detail
9. Describe the gating strategy used.	described in Material and Methods and supplementary figures

Tick this box to confirm that a figure exemplifying the gating strategy is provided in the Supplementary Information. ☒

Nature Medicine: doi:10.1038/nm.4373